

Rotational Dynamics of Discoid Colloidal Particles in Attractive Quasi-Two-Dimensional Plastic Crystals

Bing Liu,* Jiajia Zhou, and An-Chang Shi



Cite This: *J. Phys. Chem. Lett.* 2023, 14, 2402–2409



Read Online

ACCESS |



Metrics & More

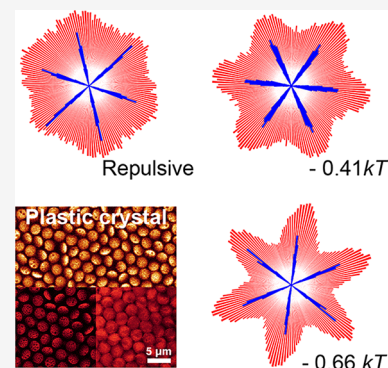


Article Recommendations



Supporting Information

ABSTRACT: Plastic crystals formed from anisotropic molecules or particles are an important state of matter characterized by the presence of long-range positional order and the lack of long-range orientational order. The rotational motion of molecules or particles in plastic crystals is the most attractive characteristic of the system. Here the rotational dynamics of the discoid particles in quasi-two-dimensional colloidal plastic crystals stabilized via depletion interactions are quantitatively studied using time-resolved confocal microscopy. The measured probability distribution of particle orientation reveals the existence of a strong coupling between the lattice symmetry and particle rotation, resulting in anisotropic rotational dynamics modes resembling the underlying hexagonal crystalline symmetry. Furthermore, the orientational distribution function provides information about the potential surface of rotational dynamics. The observed slow rotational diffusion can be attributed to the presence of orientational minima and potential barriers on the potential surface. Our findings with a real experimental system provide important insights into the role of attraction in the phase behaviors of plastic crystals.



Anisotropic molecules or particles possess positional and orientational degrees of freedom. The presence or absence of long-range order in these degrees of freedom results in different states of anisotropic particles. Liquids and crystals are states characterized by the absence and presence of both long-range positional and orientational order, respectively, whereas liquid/plastic crystals are intermediate states with and without long-range orientational order and without and with long-range positional order.^{1–3} Liquids, crystals, and liquid crystals have been studied extensively.¹ In the case of plastic crystals (PCs), it has been well established that this state of matter can occur in molecular and colloidal systems. Due to their unique properties and wide range of applications, including for high-performance polyelectrolytes, refrigeration, ferroelectric materials, and switchable nonlinear optical materials,^{4–9} PCs have attracted much attention.^{10–23} In comparison to crystalline structures, the rotational motion of molecules or particles in plastic crystals is the most distinct characteristic. However, quantitative study of the rotational dynamics of the anisotropic particles in PCs has been rare, so our understanding of the nature of the rotational dynamics modes is still very limited.

Colloidal suspensions provide a useful model system for studying the structure and dynamics of condensed matter.^{24–29} Due to the large size and slow dynamics of colloidal particles, it is possible to examine the structure and dynamics of colloidal systems using optical microscopy. Recently, the rotational diffusion of a colloidal PC was examined using confocal microscopy,¹⁶ revealing that, in the case of long-range electrostatic repulsion, the particles exhibit isotropic rotational

dynamics and free rotational diffusion. Although it is expected that the underlying crystalline symmetry due to the long-range positional order would influence the rotational dynamics of the particles, the coupling between the lattice symmetry and orientational dynamics has yet to be observed experimentally and the manner of the coupling and the extent to which such coupling could be carried out remain unclear.

To this end, we utilize the colloidal suspension of anisotropic colloidal particles as an ideal system to study the structure and dynamics of PCs. In this Letter, we report experimental results of rotational dynamics of colloidal particles in PCs with designed shapes and interparticle interactions. We use a system composed of discoid particles with tunable depletion attractions and discover that attractive interactions result in an increased level of coupling of orientational distribution to the lattice symmetry. This effect strongly influences the rotational diffusion and induces a dynamic mode transition from isotropic to anisotropic. The presence of preferred particle orientations leads to extremely slow rotational diffusion, which can further reflect the energy barriers between the minima of the potential surface.

Received: February 1, 2023

Accepted: February 27, 2023

In our experiments, we examined the structure and rotational dynamics of plastic crystals formed from colloidal discoid SiO_2 particles using quantitative confocal microscopy. The particles, consisting of a polystyrene (PS) disk and two symmetric SiO_2 spherical caps, were synthesized according to our previous work³⁰ (Figure 1a and Figure S1) and are

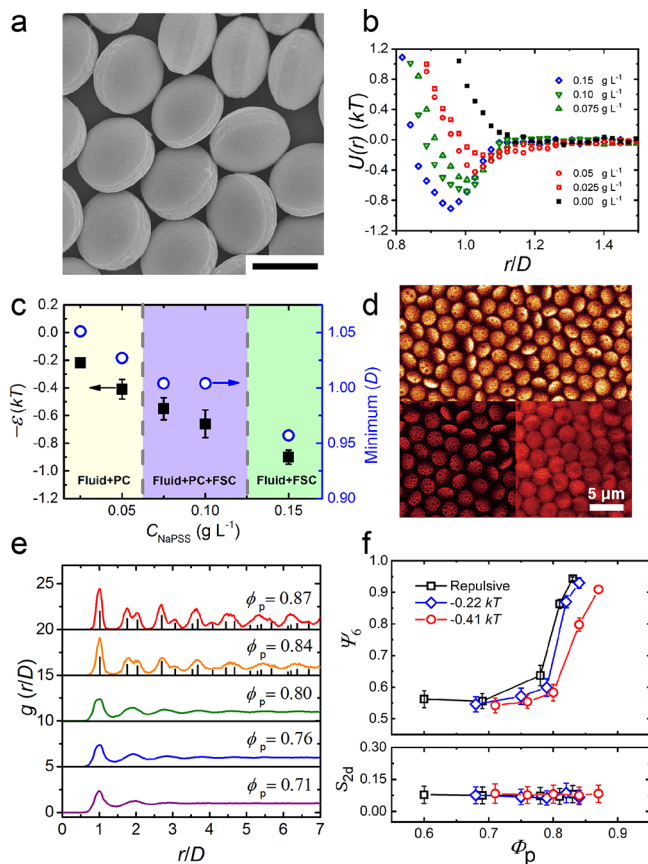


Figure 1. Pair interaction and fluid–PC transitions of discoid particles. (a) SEM image of discoid particles. The scale bar is 2 μm . (b) Pair interaction potentials that were calculated from $g(r)$ s. (c) Attraction strength (ϵ) and position of the potential minimum (r_m) as a function of C_{NaPSS} . (d) Typical CLSM image of PC of discoid particles for an ϵ of ~ 0.41 kT and corresponding superresolution image over 100 time frames (~ 43 s) (bottom right). (e) Averaged pair correlation function $g(r/D)$ for increasing ϕ_p . The black peaks are from the perfect hexagonal lattices. (f) Two-dimensional bond orientational order parameter Ψ_6 and nematic order parameter S_{2d} for increasing ϕ_p .

characterized by a length (L) of 1.80 ± 0.03 μm and a diameter (D) of 2.57 ± 0.03 μm . The aspect ratio of the particles was chosen for their ability to form plastic crystals. According to computer simulations of oblate spheroids,³¹ the discoid particles with an aspect ratio of 0.7 could form plastic crystals with hard interaction potentials. The SiO_2 particles have the symmetry of a disk or a spherocylinder. They have a negative ζ potential of approximately -40 mV (Figure S2) and are electrostatically stabilized in deionized water. The interactions between the particles are regulated by the addition of sodium polystyrenesulfonate (NaPSS), which induces a depletion force³² between the colloidal particles. The Debye length (κ^{-1}) is approximately 10–45 nm for the NaPSS concentrations ($C_{\text{NaPSS}} = 0.01$ – 0.15 g L^{-1}), as estimated by the

Debye–Hückel theory. The particle concentration is controlled such that a colloidal monolayer forms, but the particle rotation is not limited to a two-dimensional plane; thus, the experimental system is practically quasi-two-dimensional. The middle PS disk is labeled by a dye (Nile red), enabling the determination of the orientations of the particles' long axes with confocal laser scanning microscopy (CLSM) according to the projected shapes (Figure S3).

The interaction potential between the particles was obtained by inverting the pair correlation function $g(r)$ using the Ornstein–Zernike integral equation of liquid theory together with the hypernetted-chain closure equation following the method of Behrens and Grier³³ (see the Experimental Section for details). For the measurements, the particle area density (ϕ_p) ($n\pi D^2/4$, where n is the particle number) is 10%. The measured $g(r)$ s for increasing NaPSS concentrations from 0.0 to 0.15 g L^{-1} are shown in Figure S4, and the corresponding interaction potentials are shown in Figure 1b. The depth of the interaction potential well (ϵ), corresponding to the minimum of the interaction potential occurring at a distance r_m , is used as the attraction strength. Values of ϵ and r_m are plotted as a function of C_{NaPSS} in Figure 1c. The phase diagram of the system is mapped out by conducting experiments in a range of ϵ values. Three phase regions of the system have been identified for increasing ϵ : F + PC ($\epsilon \lesssim 0.5$ kT), F + PC + C (~ 0.5 $kT < \epsilon \lesssim 0.75$ kT), and F + C ($\epsilon \gtrsim 0.75$ kT), where F is the fluid state and C is the crystal state.

Plastic crystals are formed via liquid–PC transitions in samples with an attraction strength in the range of < 0.5 kT (Figure 1d; see Movies S1–S3). PCs with a large imaging area show the high quality of the formed crystals (Figure S5). The liquid–PC transitions could be regulated by areal density ϕ_p . Note that the ϕ_p could be > 1 when discoid particles tend to stand on the substrate and are close-packed because we use $\pi D^2/4$ for the area one particle takes. The benefit of using ϕ_p is that it facilitates the comparison between the self-assembled crystals of the discoid particles and those of spherical particles or discs. Above a critical value of ϕ_p , the discoid particles form an ordered structure with almost perfect hexagonal packing. An inspection of these ordered structures revealed that they possess the typical characteristics of a PC phase, that is, the presence of long-range positional order and the lack of orientational order. As a representative example, a PC phase formed at $\epsilon \lesssim 0.41$ kT is shown in Figure 1d; Figure S6 shows a full structural characterization of the samples at all of the attraction strengths. The long-range positional order is evident from the lattices and the calculated pair correlation functions $g(r)$ (Figure 1e; see Figure S7 for the tracking of the position of particles). The nature of the orientational order is studied by taking a superposition of 100 of the superresolution frames of a time series (Figure 1d). The results clearly showed that the particles orient along random directions. The calculated nematic order parameter $S_{2d} = (1/N) \sum_i^N \langle \cos(2\theta_i) \rangle$ is < 0.1 over the entire range of ϕ_p , indicating the lack of long-range orientational order by tracking the in-plane orientations [\mathbf{q} (see Figure 2a)] of the particles' long axes (see Figure S8 for the tracking of the orientations of particles). The effective lattice parameters can be extracted from the peaks in the $g(r/D)$ s of the formed PCs. Because the sample cell has a small tilt angle of $\sim 1^\circ$ from the bottom middle to the sides (Figure S3), it probably results in a gravity effect on the effective lattice parameters. However, the lattice parameters show a good agreement with the position of the pair potential minimum in

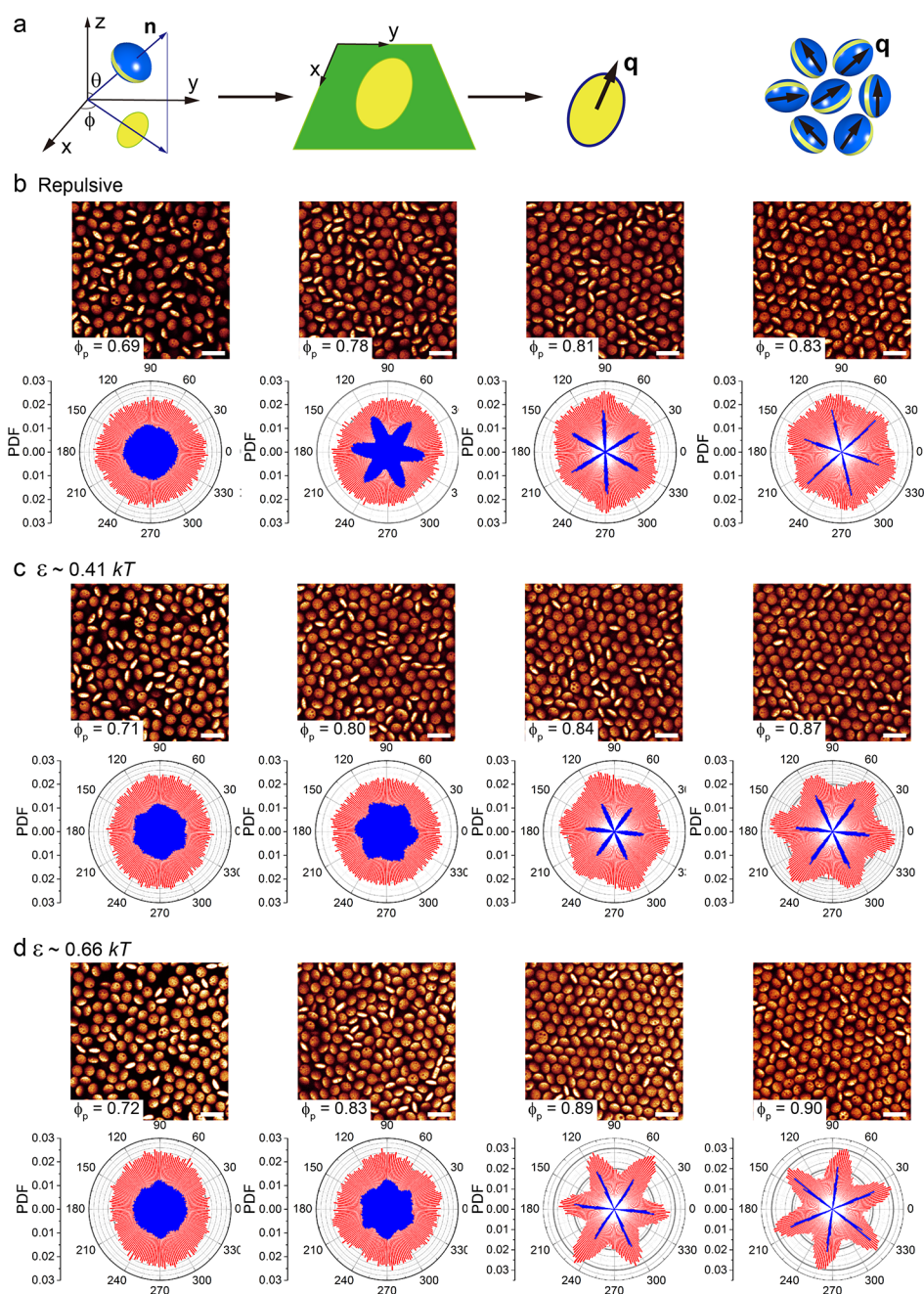


Figure 2. Hexagonally orientational distributions of long axes of discoid particles. (a) The projection of the middle disk of a particle in the image plane approximately is an ellipse, and the in-plane vector along its long axis is defined as \mathbf{q} . (b–d) Confocal microscopy images of discoid particle dispersion for increasing areal density at different attraction intensities (ϵ) and corresponding probability density function (PDF) of \mathbf{q} (red) and bond angle (blue). An arbitrary unit was used for the y -axis of the bond angle distribution. C_{NaPSS} values of (b) 0.0, (c) 0.05, and (d) 0.1 g L^{-1} . The scale bars are 5 μm .

$U(r)$ curves (Figure 1b), which is calculated from the diluted samples, suggesting that the osmotic pressure induced by gravity does not affect the lattice spacing. Furthermore, a typical PC lattice has a two-dimensional (2D) global bond orientational order parameter Ψ_6 of >0.9 (Figure 1f), confirming a highly ordered hexagonal packing.

The orientation of a discoid particle can be described by a unit vector $\mathbf{n} = \sin(\theta) \cos(\phi)\mathbf{x} + \sin(\theta) \sin(\phi)\mathbf{y} + \cos(\theta)\mathbf{z}$ that is parallel to its axial direction (Figure 2a), where the \mathbf{z} direction is chosen to be perpendicular to the plane of the quasi-two-dimensional PC. The projection of normal direction \mathbf{n} in the x – y plane is $\sin(\theta)[\cos(\phi)\mathbf{x} + \sin(\phi)\mathbf{y}]$, which is

perpendicular to in-plane vector \mathbf{q} . To quantify the rotational dynamics of the discoid particles and to elucidate the effects of the hexagonal symmetry of the lattice, we analyzed the probability density function (PDF) of in-plane orientational vector \mathbf{q} for three sets of experimental data with ϵ varying from repulsive to attractive (Figure 2b–d). For all of these ϵ values, the depletion-induced attraction between the particles and the wall does not restrict the orientation of the particles at dilute particle concentrations (Figure S9). When the particle concentrations are high enough to form PCs, the superpositioned images imply that the particles do not have restricted orientations (Figure 1d). Interestingly, the PDF

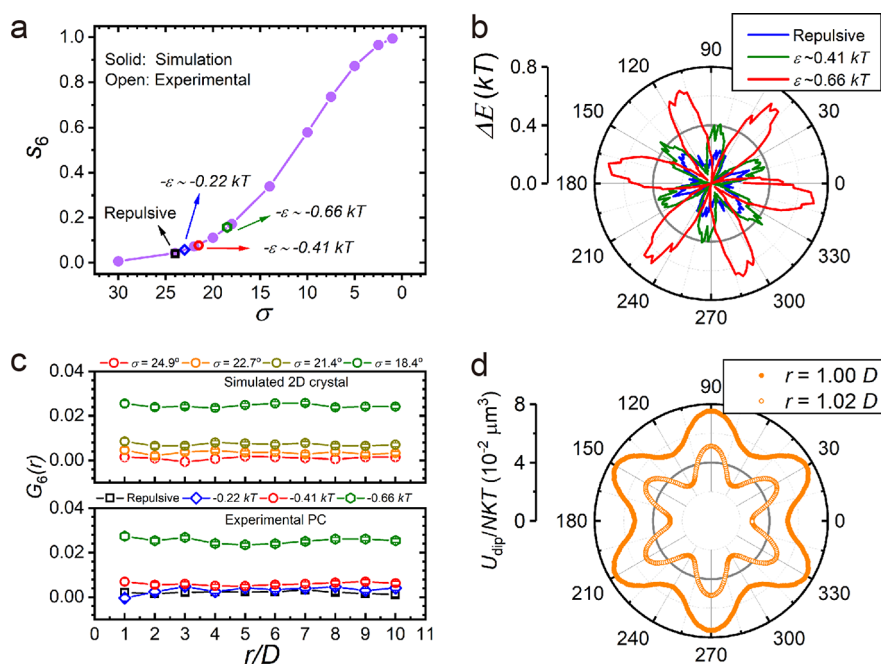


Figure 3. Quantified orientational order and angular correlation of \mathbf{q} . (a) Calculated orientational order parameter S_6 for both experimental and simulated data. σ is the standard deviation in Gaussian distributions in simulations. (b) Rotational potential barriers for particles in a hexagonal lattice. (c) Radially averaged spatial correlation $G_6(r)$ as a function of r/D . (d) Landscape of the calculated depletion potential between a central particle rotating through six freely rotating three-dimensional neighbors.

$P(\mathbf{q})$ as a function of azimuthal angle ϕ changes from an isotropic ring to a distribution with a 6-fold symmetry when ϵ is increased (Figure 2b–d), reflecting the symmetry of the underlying hexagonal lattice of the PC. This observation provides strong evidence that the lattice symmetry is coupled with the orientational distribution of the particles. Some similar coupling phenomena were reported by computer simulations in several molecular or colloidal systems,^{11,12,19–21} but it has not been observed in previous experimental studies of PCs.^{10,13–18,22,23,33,34}

To explore the origin of the emergent anisotropy in the orientational distribution, we compare and contrast the particle orientation distribution with the 2D bond angle distribution of the particles at increasing ϕ_p (Figure 2). For a given particle, the bond angle is defined as the angle between the vectors connecting its nearest neighbor particles and a reference direction. This quantity describes the crystallographic order and symmetry of the long-range ordered lattice. As expected, the liquid state of the system is characterized by the absence of structure in both the orientational and bond angle distributions. In this isotropic state, the particles have almost equal probability in all directions, although the weak peaks in the bond angle distribution are present in cases with high ϕ_p values. On the contrary, strong 6-fold peaks in the bond angle distribution are present for all PC phases. At the same time, the particle orientational distribution exhibits peaks with a 6-fold symmetry in azimuthal angle ϕ , and the peak intensity increases with ϵ (Figure 2b–d). Specifically, these peaks are very weak for the repulsive PC but become more pronounced for $\epsilon \sim 0.41$ kT and remarkably strong for $\epsilon \sim 0.66$ kT. Furthermore, the peak positions in the particle orientational distribution coincide with the peak positions in the bond angle distribution, implying that the isotropic symmetry of the rotational dynamics of the particles is broken by the lattice symmetry.

It should be noted that, although the rotational dynamics of the particles possess 6-fold symmetry, in this case, the long-range orientational order of the particles is still absent as indicated by the nematic order parameter (Figure 1f). The 6-fold symmetry of the rotation dynamics is quantified by an orientational order parameter¹³ $S_6 = (1/N) |\sum_{j=1}^N e^{i6\theta_j}|$, which is an increasing function of attraction strength ϵ , assuming values of 0 for a uniform distribution and 1 for perfect 6-fold symmetry. Experimentally, the values of S_6 are found to be 0.04, 0.06, 0.08, and 0.16 for the repulsive particles and particles with ϵ values of ~ 0.22 , ~ 0.41 , and ~ 0.66 kT, respectively (Figure 3a). This 6-fold orientational distribution suggests that the presence of neighboring particles establishes a potential surface with certain preferred directions that governs the rotational dynamics of the particles. Consequently, the rotational dynamics of the particles changes from a random walk on a unit sphere to a random walk in the potential with potential wells at the six preferred directions on the x - y plane. In particular, rotating a particle out of these preferred directions becomes an activated process with an energy barrier, which could be estimated using the Boltzmann distribution, $p_v/p_p = e^{-\Delta E/kT}$, where p_v and p_p are the probabilities in valleys and peaks, respectively (Figure 3b). Specifically, the energy barriers are estimated to be ~ 0.25 kT for repulsive particles, ~ 0.4 kT for $\epsilon \sim 0.41$ kT, and ~ 0.7 kT for $\epsilon \sim 0.66$ kT.

To obtain more insight into the rotational dynamics of discoid particles in a monolayer PC, the experimentally measured distributions of the in-plane orientations (\mathbf{q}) of discoid particles were fitted to Gaussian distributions; for the details of fittings, see the Experimental Section. The differences due to an increasing ϵ were found to be described by decreasing standard deviations σ . To perform the fitting, the six orientational peaks for each ϵ were averaged (Figure S10a,b). According to the hexagonal symmetry of the lattices, the two

neighboring orientational peaks in the orientational map can remain separated only when the distribution is within the range of $2\pi/6$. When σ is larger than $2\pi/6$, the orientational peaks overlap. This overlapping clearly affords the deviation of the fitting. To exclude this effect during fitting, the averaged orientational peak (single peak) was repeated to construct a periodic peak pattern (Figure S10c,d). To eliminate the edge effect of the pattern during the fitting as much as possible, the periods were increased to 30 (Figure S10e,f) and only the fitting values of the middle peaks were considered because the middle peaks were the least affected by the edge peaks (Tables S1–S3). When the period number is >30 , the obtained fitting values are the same. By this fitting route, we obtained four σ values of 24.9° , 22.7° , 21.4° , and 18.4° for repulsive particles and particles with ε values of ~ 0.22 , ~ 0.41 , and ~ 0.66 kT , respectively (Figures S11 and S12 and Tables S4–S6).

In experiments, a stronger attraction (>0.66 kT) resulted in a transition from PC to crystals. To explore the rotational dynamics for the cases with stronger attractions, we construct a simulated model 2D crystal. In this crystal, every particle has an in-plane orientation. Moreover, the orientational distribution displays six identical peaks that point to six neighboring particles and are Gaussian with a given σ . Because the attraction strength can be described by σ in our quasi-two-dimensional case, we changed the σ values from 0° to $\sim 30^\circ$ for this model crystal and calculated the corresponding S_6 . The calculated S_6 for each σ is shown in Figure 3a. A smaller σ resulted in a larger S_6 , implying a case of strong attraction. A larger σ resulted in a smaller S_6 , implying the crystal has more isotropic in-plane diffusion. The small difference in the S_6 values in Table 1 between the experiments and the simulated

Table 1. Comparison of S_6 Values between Experimental and Simulated Data

σ	S_6	
	experimental	simulated
18.4	0.16	0.1564
21.4	0.08	0.0819
22.7	0.06	0.042
24.9	0.04	0.0339

data again suggested that the orientational distribution of the particles' long axes can be described well by a Gaussian distribution (also see Figure 3a). The results also implied that small S_6 values in experiments are due to a wide orientational distribution, as a result of weak attractions.

To explore the nature of the emergent orientational order, the radially averaged angular correlation $G_6(r) = \langle \cos 6(\phi_r - \phi_0) \rangle$ of in-plane vector \mathbf{q} has been calculated (Figure 3c). Likewise, the $G_6(r)$ s have been calculated on the basis of both experimental and simulated 2D crystal data and are found to be comparable. In particular, both experimental and simulation $G_6(r)$ s are almost zero, indicating a very weak rotational correlation and the absence of long-range orientational order. Scrutiny of the experimental $G_6(r)$ s indicates that an increasing ε leads to a larger degree of correlation, reaching a value of ~ 0.03 for $\varepsilon \sim 0.66$ kT . However, the $G_6(r)$ stays at a small value for all of the distances examined, reflecting the nature of the plastic crystals. The effect of ε on the $G_6(r)$ s and the character of nondecay of $G_6(r)$ s can be further confirmed by the results from the data of the simulated 2D crystal (Figure 3c). The weak correlation is also confirmed by comparing the

rotational trajectories of the particles on the lattices (Figure S13). On the basis of these results, we propose a simple model for the rotational dynamics of the discoid PC monolayer, in which the rotation of the particles is modeled as a random walk on a unit sphere in the presence of a potential generated by the crystalline lattice. This model is then used to obtain the potential surface for the rotation of the particles. The resulting depletion potential landscape indeed possesses a 6-fold symmetry with six preferred orientations along crystallographic axes (Figure 3d; see Note S1 and Figure S14 for additional discussion).

For anisotropic colloids, the coupling between lattice symmetry and rotational dynamics should be quite general; therefore, an anisotropic orientational dynamic mode is expected to be found in other colloidal systems. The rotational trajectories of single particles provide more evidence for understanding the nature of rotational dynamics. Experimentally, it is observed that the in-plane rotational trajectories of single particles change from a random one to a banded one as ε is increased (Figure 4a), indicating a change from almost unhindered rotations to rotational jumps between the different preferred directions. To quantify this change, we implement an orientation analogous to the van Hove self-correlation function, $G(\phi, t) = \langle \delta[\phi - \phi_i(t)] \rangle$ for our experiments, where $\phi_i(t)$ is the angle difference between the in-plane orientation (\mathbf{q}) at times zero and t . For $\varepsilon \sim 0.66$ kT , $G(\phi, t)$ displays two separated peaks at $\sim 60^\circ$ and $\sim 120^\circ$ at a long time (86.6 s) (Figure 4b), indicating jumps between large angles. However, such peaks were not found in $G(\phi, t)$ for repulsive particles and not significant for $\varepsilon \sim 0.41$ kT . These heterogeneities in rotational dynamics will influence the rotational self-diffusion of particles. To quantify this effect, we calculated the rotational autocorrelation functions $C(t) = \langle \mathbf{p}(t) \cdot \mathbf{p}(t + \tau) \rangle$ by using in-plane orientational vector \mathbf{q} . Such a function can be correlated to rotational diffusion coefficient D_r through an equation derived by Manoharan et al.³⁴

$$\langle \mathbf{p}(t) \cdot \mathbf{p}(t + \tau) \rangle = 1/4 \sum_{l=1}^{\infty} \frac{2l+1}{l(l+1)} (S_l^1)^2 e^{-l(l+1)D_r\tau} \quad (1)$$

where $S_l^1 = \int_{-1}^1 P_l^1(x) dx$ and P_l^1 are the first order Legendre polynomials. The right side has one free parameter, D_r , which can be obtained by fitting the right side to experimental data (Figure 4c). We verified this method by using simulated data of freely diffused oblate particles (for details, see Note S2 and Figure S15). For a nonlinear fit, the goodness of fits was evaluated by the standard error of regression (SER), which reflects the average distance that the observed values fall from the regression line (for all of the evaluation of the goodness of fits, see Tables S7–S12). The SER values are listed in the caption of Figure 4. For weak attraction ($\varepsilon \lesssim 0.5$ kT), the measured curves can be described well by the equation presented above because approximately 95% of the data points lie between the regression line and ± 0.04 . For moderate attraction (0.5–0.75 kT), the obtained SER values significantly increased and the fittings gradually deviated from the equation presented above. They are better described by the Kohlrausch–Williams–Watts (KWW) function $C(t) = [\exp(-t/\tau)^\beta]$, which is used to describe the dynamics of supercooled liquids or glasses.^{35,36} The SER also reflected the difference between the two fits. When $\varepsilon \lesssim 0.5$ kT , no significant difference was observed. When $\varepsilon \gtrsim 0.5$ kT , the SER

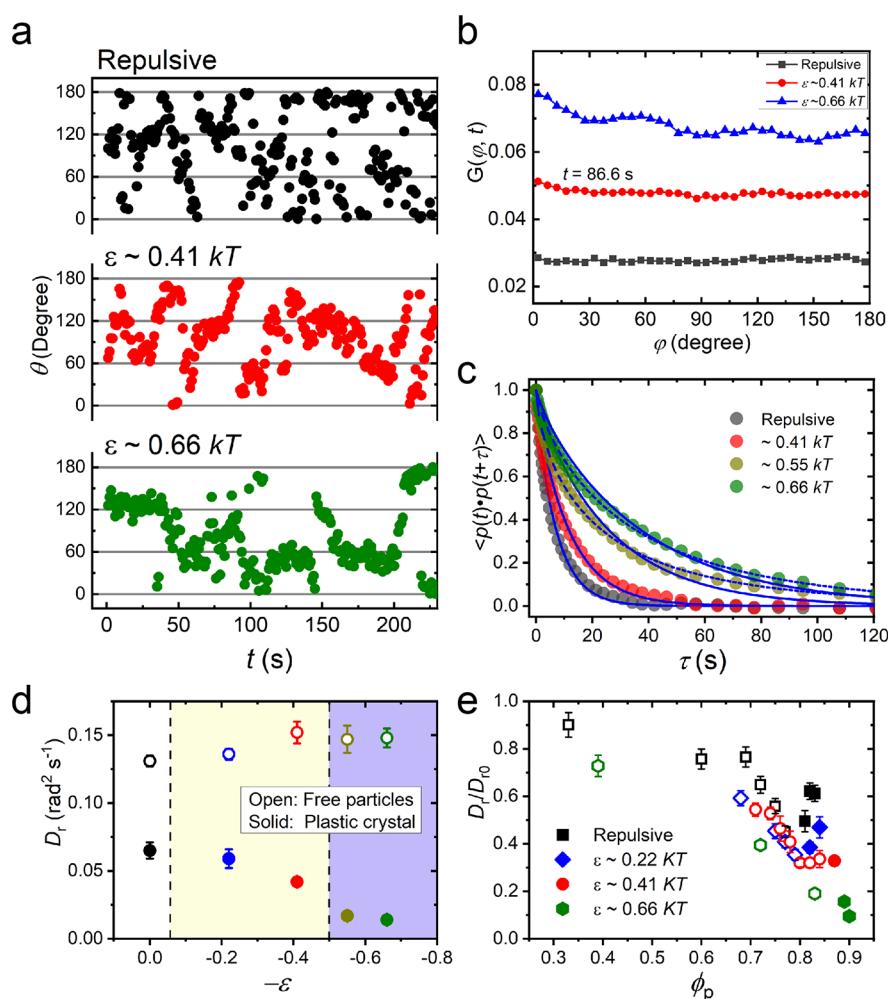


Figure 4. Rotational dynamics of orientational vector \mathbf{q} . (a) Representative rotational trajectories of vector \mathbf{q} for increasing ϵ . The gray lines are three crystallographic axes. (b) $G(\phi, t)$ function for particles in PC for an increasing ϵ at a time interval of 86.6 s. (c) Rotational autocorrelation functions of \mathbf{q} . The solid lines are the fits with eq 1, and the dashed lines are the fits with $\exp[-t/\tau]^\beta$. The standard errors of regression (SER) for the two fits are as follows. Repulsive: 0.0195, 0.0168. $\epsilon \sim 0.41 kT$: 0.0199, 0.0160. $\epsilon \sim 0.55 kT$: 0.0318, 0.0102. $\epsilon \sim 0.66 kT$: 0.0924, 0.0170. (d) Apparent rotational diffusion coefficients D_r as a function of ϵ . (e) Normalized D_r as a function of ϕ_p .

difference becomes non-negligible. We infer that this deviation is caused by the rotational jumps (Figure 4a,b).

For comparison, we still used the equation presented above to extract an apparent D_r for all interactions. From the measurements, all particles in the PC phases exhibit a rotational relaxation remarkably slower than that of the very diluted particles (Figure 4d). For an increasing ϵ , the degree of deceleration becomes more pronounced, and D_r/D_0 (D_0 is the D_r of the very diluted particles) decreases from 0.61 for repulsive particles to 0.33 for $\epsilon \sim 0.41 kT$ and 0.10 for $\epsilon \sim 0.66 kT$. The results are in sharp contrast to those for the completely freely rotating rods on body-centered cubic PCs.¹⁶ No evidence shows that gravity compression affects the measured D_r values (Figure S15d). The decrease in D_r/D_0 for increasing ϕ_p is depicted in Figure 4e. As expected from hard spheres,^{37,38} the D_r/D_0 of uncrystallized particles gradually decreases as ϕ_p increases. Once particles form crystals, a faster D_r/D_0 is expected due to the structural difference. This could be the case for weak attractions ($\epsilon \sim 0.22 kT$). D_r/D_0 continuously decreases with an increasing ϵ (0.41–0.66 kT), which should be attributed to the significant contribution of attraction. For a stronger attraction ($\epsilon > 0.75 kT$), the rotational motion of particles was completely frozen

due to a first-order PC–crystal transition.²³ Because the studied PC monolayer is near the substrate, the substrate might have an influence on the rotational dynamics of particles, and further study is needed to clarify this effect.

In summary, the rotational dynamics of anisotropic particles in a plastic crystal formed from discoid particles have been quantitatively studied using confocal microscopy. We have discovered that the rotational dynamics of the discoid particles strongly couples to the lattice symmetry. The coupling effect depends sensitively on the attraction strength of the interparticle interactions and could be modeled as a random walk on a unit sphere with certain anisotropic potential. The symmetry of the potential surface is dictated by the crystalline lattice, resulting in preferred orientations of the particle directors, although the system still lacks long-range orientational order. The presence of preferred particle orientations leads to extremely slow rotational diffusion of the particles due to the energy barriers between the minima of the potential surface. The results for plastic crystals can be further extended to tune colloidal interaction to manipulate or even create orientational order and rotational dynamics of plastic crystals for applications.

ASSOCIATED CONTENT

Supporting Information

The Supporting Information is available free of charge at <https://pubs.acs.org/doi/10.1021/acs.jpcllett.3c00299>.

Experimental Section, definition of order parameters, particle tracking, measurement of pair potentials, Gaussian fitting, computer simulations and calculations, 15 supporting figures, 12 supporting tables, and descriptions of Movies S1–S3 (PDF)

Plastic crystals of repulsive particles (Movie S1) (AVI)

Plastic crystals of attractive particles with an attraction strength $\varepsilon = 0.41$ kT (Movie S2) (AVI)

Plastic crystals of attractive particles with an attraction strength $\varepsilon = 0.66$ kT (Movie S3) (AVI)

AUTHOR INFORMATION

Corresponding Author

Bing Liu – Beijing National Laboratory for Molecular Sciences, State Key Laboratory of Polymer Physics and Chemistry, Institute of Chemistry, Chinese Academy of Sciences, Beijing 100190, China; orcid.org/0000-0003-4297-157X; Email: liubing@iccas.ac.cn

Authors

Jiajia Zhou – South China Advanced Institute for Soft Matter Science and Technology, School of Emergent Soft Matter, South China University of Technology, Guangzhou, Guangdong 510640, China; orcid.org/0000-0002-2258-6757

An-Chang Shi – Department of Physics and Astronomy, McMaster University, Hamilton, Ontario, Canada L8S 4M1

Complete contact information is available at: <https://pubs.acs.org/doi/10.1021/acs.jpcllett.3c00299>

Notes

The authors declare no competing financial interest.

ACKNOWLEDGMENTS

The authors thank Dr. Jiawei Lu for the synthesis of discoid particles and Prof. Bing Miao at UCAS for the helpful discussions. The research was supported by NSFC (22172175) and the Hundred Talents Program of ICCAS. A.-C.S. acknowledges the support from the Natural Sciences and Engineering Research Council (NSERC) of Canada.

REFERENCES

- (1) Chaikin, P. M.; Lubensky, T. C. *Principles of condensed matter physics*; Cambridge University Press: Cambridge, U.K., 1995.
- (2) Timmermans, J. Plastic crystals: A historical review. *J. Phys. Chem. Solids* **1961**, *18*, 1–8.
- (3) Sherwood, J. *The plastically crystalline state: Orientationally disordered crystals*; John Wiley: New York, 1979.
- (4) Alarco, P. J.; Abu-Lebdeh, Y.; Abouimrane, A.; Armand, M. The plastic-crystalline phase of succinonitrile as a universal matrix for solid-state ionic conductors. *Nat. Mater.* **2004**, *3*, 476–81.
- (5) Basile, A.; Hilder, M.; Makhlooghiazad, F.; Pozo-Gonzalo, C.; MacFarlane, D. R.; Howlett, P. C.; Forsyth, M. Ionic liquids and organic ionic plastic crystals: advanced electrolytes for safer high performance sodium energy storage technologies. *Adv. Energy Mater.* **2018**, *8*, 1703491.
- (6) Li, B.; et al. Colossal barocaloric effects in plastic crystals. *Nature* **2019**, *567*, 506–510.

(7) Cazorla, C. Refrigeration based on plastic crystals. *Nature* **2019**, *567*, 470–471.

(8) Harada, J.; Shimojo, T.; Oyamaguchi, H.; Hasegawa, H.; Takahashi, Y.; Satomi, K.; Suzuki, Y.; Kawamata, J.; Inabe, T. Directionally tunable and mechanically deformable ferroelectric crystals from rotating polar globular ionic molecules. *Nat. Chem.* **2016**, *8*, 946–952.

(9) Sun, Z.; Chen, T.; Liu, X.; Hong, M.; Luo, J. Plastic transition to switch nonlinear optical properties showing the record high contrast in a single-component molecular crystal. *J. Am. Chem. Soc.* **2015**, *137*, 15660–15663.

(10) Das, S.; Mondal, A.; Reddy, C. M. Harnessing molecular rotations in plastic crystals: a holistic view for crystal engineering of adaptive soft materials. *Chem. Soc. Rev.* **2020**, *49*, 8878–8896.

(11) Vega, C.; Paras, E. P. A.; Monson, P. A. Solid–fluid equilibria for hard dumbbells via monte carlo simulation. *J. Chem. Phys.* **1992**, *96*, 9060–9072.

(12) Aragoes, J. L.; Conde, M. M.; Noya, E. G.; Vega, C. The phase diagram of water at high pressures as obtained by computer simulations of the TIP4P/2005 model: the appearance of a plastic crystal phase. *Phys. Chem. Chem. Phys.* **2009**, *11*, 543–55.

(13) Shen, W.; Antonaglia, J.; Anderson, J. A.; Engel, M.; van Anders, G.; Glotzer, S. C. Symmetries in hard polygon systems determine plastic colloidal crystal mesophases in two dimensions. *Soft Matter* **2019**, *15*, 2571–2579.

(14) Gantapara, A. P.; de Graaf, J.; van Rooij, R.; Dijkstra, M. Phase behavior of a family of truncated hard cubes. *J. Chem. Phys.* **2015**, *142*, 054904.

(15) Karas, A. S.; Dshemuchadse, J.; van Anders, G.; Glotzer, S. C. Phase behavior and design rules for plastic colloidal crystals of hard polyhedra via consideration of directional entropic forces. *Soft Matter* **2019**, *15*, 5380–5389.

(16) Liu, B.; Besseling, T. H.; Hermes, M.; Demirörs, A. F.; Imhof, A.; van Blaaderen, A. Switching plastic crystals of colloidal rods with electric fields. *Nat. Commun.* **2014**, *5*, 3092.

(17) Meijer, J. M.; Crassous, J. J. Phase behavior of bowl-shaped colloids: order and dynamics in plastic crystals and glasses. *Small* **2018**, *14*, 1802049.

(18) Meijer, J.-M.; Pal, A.; Ouhajji, S.; Lekkerkerker, H. N. W.; Philipse, A. P.; Petukhov, A. V. Observation of solid-solid transitions in 3d crystals of colloidal superballs. *Nat. Commun.* **2017**, *8*, 14352.

(19) Chu, F.; Heptner, N.; Lu, Y.; Siebenbürger, M.; Lindner, P.; Dzubiella, J.; Ballauff, M. Colloidal plastic crystals in a shear field. *Langmuir* **2015**, *31*, 5992–6000.

(20) Liu, B.; Besseling, T. H.; van Blaaderen, A.; Imhof, A. Confinement induced plastic crystal-to-crystal transitions in rodlike particles with long-ranged repulsion. *Phys. Rev. Lett.* **2015**, *115*, 078301.

(21) Vutukuri, H. R.; Imhof, A.; van Blaaderen, A. Fabrication of polyhedral particles from spherical colloids and their self-assembly into rotator phases. *Angew. Chem., Int. Ed.* **2014**, *53*, 13830–13834.

(22) Hosein, I. D.; John, B. S.; Lee, S. H.; Escobedo, F. A.; Liddell, C. M. Rotator and crystalline films via self-assembly of short-bond-length colloidal dimers. *J. Mater. Chem.* **2009**, *19*, 344–349.

(23) Lu, J.; Bu, X.; Zhang, X.; Liu, B. Self-assembly of shape-tunable oblate colloidal particles into orientationally ordered crystals, glassy crystals and plastic crystals. *Soft Matter* **2021**, *17*, 6486–6494.

(24) Poon, W. Colloids as big atoms. *Science* **2004**, *304*, 830–831.

(25) Pusey, P. N.; van Meegen, W. Phase behaviour of concentrated suspensions of nearly hard colloidal spheres. *Nature* **1986**, *320*, 340–342.

(26) Hwang, H.; Weitz, D. A.; Spaepen, F. Direct observation of crystallization and melting with colloids. *Proc. Natl. Acad. Sci. U.S.A.* **2019**, *116*, 1180–1184.

(27) Peng, Y.; Wang, F.; Wang, Z.; Alsayed, A. M.; Zhang, Z.; Yodh, A. G.; Han, Y. Two-step nucleation mechanism in solid-solid phase transitions. *Nat. Mater.* **2015**, *14*, 101–108.

(28) Tan, P.; Xu, N.; Xu, L. Visualizing kinetic pathways of homogeneous nucleation in colloidal crystallization. *Nat. Phys.* **2014**, *10*, 73–79.

(29) Yethiraj, A.; van Blaaderen, A. A colloidal model system with an interaction tunable from hard sphere to soft and dipolar. *Nature* **2003**, *421*, 513–517.

(30) Luo, Z.; Liu, B. Shape-tunable colloids from structured liquid droplet templates. *Angew. Chem., Int. Ed.* **2018**, *57*, 4940–4945.

(31) Odriozola, G. Revisiting the phase diagram of hard ellipsoids. *J. Chem. Phys.* **2012**, *136*, 134505.

(32) Asakura, S.; Oosawa, F. On interaction between two bodies immersed in a solution of macromolecules. *J. Chem. Phys.* **1954**, *22*, 1255–1256.

(33) Behrens, S. H.; Grier, D. G. Pair interaction of charged colloidal spheres near a charged wall. *Phys. Rev. E* **2001**, *64*, 050401.

(34) Wang, A.; Dimiduk, T. G.; Fung, J.; Razavi, S.; Kretschmar, I.; Chaudhary, K.; Manoharan, V. N. Using the discrete dipole approximation and holographic microscopy to measure rotational dynamics of non-spherical colloidal particles. *J. Quant. Spectrosc. Radiat. Transfer* **2014**, *146*, 499–509.

(35) Jiang, S.; Yan, J.; Whitmer, J. K.; Anthony, S. M.; Luijten, E.; Granick, S. Orientationally glassy crystals of janus spheres. *Phys. Rev. Lett.* **2014**, *112*, 218301.

(36) Cicerone, M. T.; Blackburn, F. R.; Ediger, M. D. How do molecules move near T_g? Molecular rotation of six probes in o-terphenyl across 14 decades in time. *J. Chem. Phys.* **1995**, *102*, 471–479.

(37) Degiorgio, V.; Piazza, R.; Jones, R. B. Rotational diffusion in concentrated colloidal dispersions of hard spheres. *Phys. Rev. E* **1995**, *52*, 2707–2717.

(38) Hagen, M. H. J.; Frenkel, D.; Lowe, C. P. Rotational diffusion in dense suspensions. *Physica A* **1999**, *272*, 376–391.

Recommended by ACS

Fully Dispersed IrO_x Atomic Clusters Enable Record Photoelectrochemical Water Oxidation of Hematite in Acidic Media

Shao-Yu Yuan, Jian-Jun Wang, *et al.*

FEBRUARY 28, 2023
NANO LETTERS

READ 

Experimental Observation of the Spontaneous Emission of a Space–Time Wavepacket in a Multimode Optical Fiber

Karolina Stefańska, Bertrand Kibler, *et al.*

FEBRUARY 21, 2023
ACS PHOTONICS

READ 

Room-Temperature Polaron-Mediated Polariton Nonlinearity in MAPbBr₃ Perovskites

Mikhail A. Masharin, Ivan A. Shelykh, *et al.*

FEBRUARY 14, 2023
ACS PHOTONICS

READ 

Level Attraction due to Dissipative Phonon–Phonon Coupling in an Opto-Mechano-Fluidic Resonator

Qijing Lu, Shusen Xie, *et al.*

FEBRUARY 16, 2023
ACS PHOTONICS

READ 

Get More Suggestions >